

## $\beta$ -Cyclodextrin-grafted hyaluronic acid as a supramolecular polysaccharide carrier for cell-targeted drug delivery

Parbeen Singh <sup>a,b,c,1</sup>, Yongli Chen <sup>a,b,1</sup>, Deependra Tyagi <sup>d</sup>, Li Wu <sup>c</sup>, Xiaohong Ren <sup>c</sup>, Jinglong Feng <sup>a</sup>, Andrew Carrier <sup>e</sup>, Tiangang Luan <sup>b</sup>, Yongjun Tang <sup>a,\*</sup>, Jiwen Zhang <sup>c,f,\*</sup>, Xu Zhang <sup>e,\*</sup>

<sup>a</sup> Postdoctoral Innovation Practice Base, Department of Biological Applied Engineering, Shenzhen Key Laboratory of Fermentation, Purification and Analysis, Shenzhen Polytechnic, Shenzhen 518055, China

<sup>b</sup> State Key Laboratory Biocontrol, School of Marine Sciences, Sun Yat-sen University, Guangzhou 51027, China

<sup>c</sup> Center for Drug Delivery Systems, Shanghai Institute of Materia Medica, Chinese Academy of Sciences, Shanghai 201203, China

<sup>d</sup> School of Basic Medical Sciences, School of Medicine, Shenzhen University, Shenzhen, Guangdong 518060, China

<sup>e</sup> Department of Chemistry and Department of Health Sciences, Cape Breton University, 1250 Grand Lake Road, Sydney, Nova Scotia B1P 6L2, Canada

<sup>f</sup> NMPA Key Laboratory for Quality Research and Evaluation of Pharmaceutical Excipients, National Institutes for Food and Drug Control, No.2 Tiantan Xili, Beijing 100050, China



### ARTICLE INFO

#### Keywords:

Targeted drug delivery  
Supramolecular polymer  
Hyaluronic acid-cyclodextrin  
pH-responsive drug release

### ABSTRACT

$\beta$ -Cyclodextrin ( $\beta$ -CD) was grafted onto hyaluronic acid (HA) in a single step to generate a supramolecular biopolymer (HA- $\beta$ -CD) that was explored for targeted drug delivery applications. Along with its excellent biocompatibility, the prepared HA- $\beta$ -CD exhibits not only exceptionally high loading capacity for the model drugs doxorubicin and Rhodamine B through the formation of inclusion complexes with the  $\beta$ -CD component, but also the capability of targeted drug delivery to cancerous cells with a high level of expression of CD44 receptors, attributable to its HA component. The polymer can release the drug under slightly acidic conditions. With all its attributes, HA- $\beta$ -CD may be a promising cancer-cell-targeting drug carrier.

### 1. Introduction

Conventional tissue-targeting drug carriers are limited by their suboptimal selectivity in organ- or tissue-specific accumulation and retention, premature drug release and metabolism during systemic circulation, and cytotoxicity, e.g., when using unstable silver and other inorganic nanoparticles (Liechty et al., 2010; Liu et al., 2018). Drug delivery research is currently focused on achieving a good therapeutic index using more biocompatible materials (Ekladious et al., 2019; Li et al., 2019; Mao et al., 2018; Miraftab and Xiao, 2019; Yan et al., 2017). Supramolecular polymers are advanced drug carriers that target specific sites with tunable drug release (Webber et al., 2016). They form non-covalent inclusion complexes with various molecules based on specific, directional, and reversible non-covalent interactions. Additionally, they can be used to develop supramolecular biomaterials that respond to physical cues or participate in biological signaling processes (Langer and

Vacanti, 1993; Webber et al., 2015). With the advancement of drug carrier development, supramolecular grafted polymers have become preferred materials for biomedical, tissue engineering, and drug delivery applications (Namgung et al., 2014).

Hyaluronic acid (HA) is a glycosaminoglycan and a major constituent of the extracellular matrix (Laurent, 1989). It is essential for tissue organization, cell growth, adhesion, proliferation, migration, differentiation, and organ structure stability (Entwistle et al., 1996; Hua et al., 1993; Knudson and Knudson, 1993). HA binds to CD44 and RHAMM receptors that are overexpressed by tumor cells (Hall et al., 1995; Herrlich et al., 1998). Its targeting ability, biodegradability, and tissue engineering applications are well documented (Ahrens et al., 2001; Choi et al., 2011; Yu et al., 2013). Cyclodextrins (CDs) are biocompatible, amphiphilic, cyclic oligomeric supramolecules that can form inclusion complexes with small molecules. CDs have been used to form a multi-stimuli responsive supramolecular assembly for various biological

\* Corresponding authors at: Center for Drug Delivery Systems, Shanghai Institute of Materia Medica, Chinese Academy of Sciences, No. 501 of Haik Road, Shanghai 201203, China (J. Zhang).

E-mail addresses: [tangyongjun@szpt.edu.cn](mailto:tangyongjun@szpt.edu.cn) (Y. Tang), [jwzhang@simm.ac.cn](mailto:jwzhang@simm.ac.cn) (J. Zhang), [Xu\\_Zhang@cbu.ca](mailto:Xu_Zhang@cbu.ca) (X. Zhang).

<sup>1</sup> These authors contributed equally.

actions (Davis and Brewster, 2004). Among them,  $\beta$ -CD is the most investigated excipient for pharmaceutical applications that enhance the physicochemical profiles of guest molecules through its formation of inclusion complexes (Crini, 2014). Also,  $\beta$ -CD and its polymer derivatives enhance the water solubility and bioavailability of hydrophobic drugs (Zhou and Ritter, 2010). Although various polysaccharide polymers have been exploited for drug delivery applications, such as dextran (Xiao et al., 2020), CDs are preferred because they have many important attributes for drug delivery, such as high encapsulation efficiency, easy availability, and solubility enhancement properties.

Fabricating polymers with targeting moieties is a major step in the development of targeted drug delivery systems (Lv et al., 2010; Orive et al., 2009; Wang et al., 2016). CD and HA molecules may exhibit synergistic effects when exploited as a grafted supramolecular biopolymer. HA has multiple functional groups that were used to couple with the free hydroxy groups of  $\beta$ -CD (Lee et al., 2009; Lee et al., 2011). Although synthesis of  $\beta$ -CD-grafted HA has been reported (Charlot et al., 2006; Ji et al., 2017; Soltés et al., 1999), these methods were complicated and time-consuming, limiting its translation to industrial and clinical applications. Recently, we reported a single-step chemical conjugation of CD with HA (Singh et al., 2020). The synthesized HA- $\beta$ -CD has excellent water solubility enhancement of tocopherol. In this work, we further demonstrate its excellent property for the targeted delivery of chemotherapeutic agents. The drug delivery relevant properties including drug loading, controlled release, biocompatibility, and selective cell targeting were systematically investigated, demonstrating its promise as a target responsive drug carrier.

## 2. Experimental section

### 2.1. Materials

$\beta$ -Cyclodextrin ( $\beta$ -CD) was purchased from Anhui Sunhere Pharmaceutical Excipients Co., Ltd. (Shanghai, China). Hyaluronic acid sodium salt (average molecular weight 27,000 Da) was purchased from Shandong Topscience Biotech Co., Ltd. (Qingdao, China). Diphenyl carbonate (DPC, >99.9% purity) was purchased from Shanghai Aladdin Bio-Chem Technology Co., Ltd. (Shanghai, China). Rhodamine B, triethylamine (TEA), dimethylformamide (DMF), and ethanol (EtOH) were purchased from Sinopharm Chemical Reagent Co., Ltd. (Shanghai, China). All chemicals and reagents used were of analytical grade and used without further purification. Doxorubicin (Dox) (>99.5% purity) was purchased from Dalian Meilun Biotech Co., Ltd. (Dalian, China). HeLa, MCF-7, and A549 cells were obtained from the Chinese Academy of Sciences (Shanghai, China). Dulbecco's modified Eagle's medium (DMEM) and fetal bovine serum (FBS) were purchased from Thermo Fisher Scientific Ltd. (Shanghai, China). The cell labeling dye, DAPI H-1200, was purchased from Vector Laboratories Inc. (Burlingame, CA, USA). An FITC annexin V apoptosis detection kit was purchased from BD Bioscience (Franklin Lakes, NJ, USA). The primary antibodies and secondary antibodies for Western blotting analysis were purchased from Cell Signaling Technology (Danvers, MA, USA). A SuperSignal West Pico Chemiluminescent kit was purchased from Pierce Chemical Co. (Rockford, IL, USA). A Cell Cycle and Apoptosis Analysis Kit was obtained from Beyotime Biotech. Co. (Beijing, China). [ $^{13}\text{C}, ^2\text{H}_3$ ]-doxorubicin trifluoroacetate was obtained from Merck (Kenilworth, NJ, USA).

### 2.2. HA- $\beta$ -CD synthesis and characterization

HA was coupled to  $\beta$ -CD using diphenyl carbonate (DPC) as the crosslinker using our previously reported procedure (Singh et al., 2020) (Fig. S1). Briefly, a solution containing 60 mM each of  $\beta$ -CD and HA in DMF (10 mL) was heated to 80 °C, and then DPC (120 mM) was added and stirred for 15 min. Afterward, triethylamine (TEA, 300  $\mu$ L) was added to catalyze the reaction, which continued for 12 h. The reaction solution was then cooled to ambient temperature and diluted with six

volumes of ethanol to yield a precipitate, which was centrifuged (4000 rpm for 10 min) and rinsed with ethanol to remove the phenol byproduct and other impurities. Finally, the synthesized HA- $\beta$ -CD was thoroughly washed with acetone followed by ethanol (Soxhlet extraction, 8 h) before drying *in vacuo* overnight at 45 °C.  $^1\text{H}$  NMR analysis was performed on a Bruker 400 MHz Avance spectrometer. Polymer samples were dissolved in  $\text{D}_2\text{O}$  whereas  $\beta$ -CD was dissolved in  $\text{CDCl}_3$ . Surface hydrophilicity was determined by measuring the water contact angle. The bulk morphology was assessed using scanning electron microscopy (SEM, S3400, Hitachi, Tokyo, Japan). The specimens were immobilized on a metal stub with double-sided adhesive tape and sputter-coated with a thin gold film before observing under definite magnification.

### 2.3. Surface area and porosity of HA- $\beta$ -CD powder

The surface area and porosity of the samples were measured through nitrogen physisorption by Brunauer–Emmett–Teller (BET) analysis (TriStar 3000 V6.05 A, Perkin Elmer, Waltham, MA, USA). Before analysis, samples were activated by immersing in dichloromethane for 3 d and drying *in vacuo* at 50 °C for 12 h. Samples were degassed under vacuum ( $10^{-5}$  Torr) at 100 °C for 5 h.

### 2.4. Molecular weight and polydispersity

The molecular weight and polydispersity were measured using high-performance gel permeation chromatography (HPGPC, Agilent 1260 Chem station, Agilent, Santa Clara, CA, USA) equipped with UV and refractive index detectors and two tandem columns (ks802 and ks804). The columns were calibrated using dextran standards, i.e., T-700, T-580, T-500, T-110, T-80, T-70, T-40, T-11, T-9.3, and T-4 series, to generate a standard curve. The mobile phase was 0.1 M  $\text{NaNO}_3$  prepared with filtered and degassed MilliQ water at a flow rate of 0.5 mL min $^{-1}$ , and the column temperature was 40 °C. Known amounts of samples (~2–3 mg) were dissolved in 500  $\mu$ L of the mobile phase, centrifuged 10 min, and passed through a 0.22  $\mu$ m membrane filter. The column was equilibrated for 3–4 h, and 20  $\mu$ L aliquots of sample solutions were injected in triplicate. The HA and HA- $\beta$ -CD samples were injected and run for 40 min.

### 2.5. Drug loading

The HA- $\beta$ -CD drug loading experiment was performed by dissolving 100 mg of HA- $\beta$ -CD powder in 20 mL of 0.5 mg mL $^{-1}$  of either Dox or Rhodamine B in ethanol and agitating with a horizontal shaker (100 rpm) at ambient temperature for 8 h. After 8 h of incubation, the precipitate was centrifuged and dried *in vacuo*. The drug encapsulation efficiency of the polymers was determined by measuring the amount of drug released in water from 5 mg of drug-loaded polymer powder after centrifugation, where the supernatant was collected and analyzed using high-performance liquid chromatography (HPLC).

Dox and Rhodamine B were quantified using an Agilent 1290 infinity series HPLC equipped with a Gemini C18 column (4.6 mm × 150 mm × 5  $\mu$ m particle size). For Dox, the mobile phase was isocratic 0.1% trifluoroacetic acid in  $\text{H}_2\text{O}$  and MeOH (50:50), whereas for Rhodamine B the mobile phase was isocratic 70:30 MeOH: $\text{H}_2\text{O}$ . The flow rate was 1.0 mL min $^{-1}$  for both. The column temperatures were 35 and 25 °C for Dox and Rhodamine B, respectively. Dox and Rhodamine B were monitored at  $\lambda_{\text{max}} = 233$  and 550 nm, respectively. Injection volumes of 10  $\mu$ L were used and the methods were calibrated using least-squares regression of the nominal concentrations of standard solutions versus the peak area.

### 2.6. pH-dependent drug release

To determine the drug release profile of Dox-loaded HA- $\beta$ -CD samples, different release media were used, i.e., pH 1.2 HCl, pH 4.5 acetate buffer, pH 6.5 phosphate buffer, and pH 7.4 phosphate buffer. Briefly,

10 mg Dox-equivalent samples were dissolved in 100 mL of the buffer solutions by using a dissolution apparatus (Distek, North Brunswick, NJ, USA) with USP apparatus-2 (paddle) at 37 °C. At predetermined intervals, 0.5 mL of the solutions were removed for HPLC analysis and replenished with fresh buffer. The amount of Dox released was determined by HPLC. Each experiment was performed in triplicate.

### 2.7. Cytotoxicity test

HeLa, MCF-7, and A549 cell lines were cultured in DMEM medium supplemented with 10% fetal bovine serum (FBS), 100 U/mL of penicillin, and 100 µg/mL of streptomycin and incubated at 37 °C in a humidified 5% CO<sub>2</sub> atmosphere. The medium was changed every 2 d during incubation. Cells were collected from the exponentially growing phase for cytotoxicity testing and cellular uptake experiments, as detailed below. Cell enumeration was performed with the counting chamber method.

The *in vitro* cytotoxicity of HA-β-CD was tested using the HeLa cell line with an Enhanced Cell Counting Kit-8 (CCK-8, Beyotime, Shanghai). HeLa cells were seeded into 96-well plates (3000 cells/well) and incubated for 12 h. Afterward, the cells were treated with different concentrations of drug samples along with positive and negative controls for 12, 24, and 48 h. Subsequently, the CCK-8 solution (10 µL) was added to each well and incubated for 3 h. In each study, test samples and controls were evaluated in triplicate. Cell viability was expressed as light absorbance relative to that of the untreated control. The absorbance was measured at 450 nm using a microplate reader (Multiscan Go, Thermo Scientific, Waltham, MA, USA). The cell viability was calculated by using the following formula (1):

$$\text{Cell Viability}(\%) = \frac{\text{OD}_{\text{exp}} - \text{OD}_{\text{blank}}}{\text{OD}_{\text{control}} - \text{OD}_{\text{blank}}} \times 100 \quad (1)$$

where OD<sub>exp</sub>, OD<sub>blank</sub>, and OD<sub>control</sub> were the absorbances of the sample, blank, and control experiments, respectively.

### 2.8. Determination of CD44 expression on cancer cells

Flow cytometry analysis was performed to determine the CD44 expression in different cancer cells. Three cell lines with various levels of CD44 expression, i.e., A549, HeLa, and MCF-7 cells (5x10<sup>4</sup>) were used for flow cytometry measurement. Cells were seeded onto a culture plate for 24 h, the culture medium was removed, and the cells were washed with PBS. Then 10<sup>5</sup> cells were freshly suspended in 1 mL of cold PBS in flow cytometer tubes. Fluorescein isothiocyanate (FITC) anti-human CD44 antibodies were added and incubated at 4 °C for 30 min. Cells without added antibodies were used as the control.

### 2.9. Selective cellular uptake

To determine the selective targeting properties of HA-β-CD, a cellular uptake study was performed on HeLa and MCF-7 cells. The cells were seeded onto glass-bottom dishes (35 mm, NEST) at 5000 cells/dish and cultured overnight. To check the intracellular localization of HA-β-CD particles, Rhodamine B and Dox-loaded HA-β-CD were incubated with cells for 4 h. Afterward, the cells were stained with DAPI H1200 to identify the lysosomes and nuclei. Intracellular localization of samples was recorded using confocal laser scanning microscopy (CLSM, Leica DMi8, Wetzlar, Germany) and confocal images were processed by LAS-X software. All the cell experiments were performed in triplicate. Rhodamine B and Dox yield green and red fluorescence, respectively.

### 2.10. Apoptosis and cell cycle distribution study

To investigate the potential apoptotic effect of the samples, HeLa cells were exposed to Dox-loaded HA-β-CD polymer, HA-β-CD polymer

without Dox, and free Dox (positive control) in parallel with negative control (PBS buffer) for 24 h. Then the treated HeLa cells were washed with ice-cold PBS and harvested in 6 well plates. Afterward, the cells were stained using an annexin V-FITC/PI cell apoptosis kit as per the manufacturer's instructions. The cell viability percentage was checked by a flow cytometer (Beckman Coulter, Brea, CA, USA). Also, the untreated and treated HeLa cells (1 × 10<sup>6</sup>/mL) were rinsed with ice-cold PBS before suspending in 1 mL of ice-cold 70% ethanol for 12 h at 4 °C. The fixed cells were spun down and stained with propidium iodide (Beyotime Biotech, Shanghai, China) for 30 min at 37 °C in the dark before flow cytometry analysis.

Furthermore, a Western blotting test was performed to evaluate the cleaved poly(ADP-ribose) polymerase (PARP) during apoptosis. The treated and untreated HeLa cells were washed with ice-cold PBS twice and then scraped with a cell scraper. The cell proteins were acquired by the addition of ice-cold lysis buffer (10 mM HEPES (pH 7.9), 10 mM KCl, 1 mM EDTA, and 0.1% NP-40) including freshly prepared protease inhibitor cocktails into the cells. Protein concentration in the supernatant of the lysate was quantified using a bicinchoninic acid (BCA) protein kit. Afterward, 20 µg of cell proteins were applied to 12% sodium dodecyl sulfate (SDS)-polyacrylamide gel electrophoresis (PAGE) for protein separation followed by semi-dry electrophoretic transfer to PVDF membranes at 20 V for 60 min. After blocking the membranes in 5% (w/v) bovine serum albumin (BSA) for 2 h, the membranes were incubated with an anti-cleaved PARP primary antibody (1:1000) at 4 °C overnight. The immunoreactive bands were detected by an HRP-conjugated secondary antibody (1:3000) hybridization, and protein bands were visualized by an imaging system (Bio-Rad, Munich, Germany) using the SuperSignal West Pico Chemiluminescent Substrate kit (Millipore Corporation, Billerica, MA, USA) according to the manufacturer's instructions. β-actin was used as a loading control for the total protein content and showed no differences between groups.

### 2.11. Pharmacokinetic study

All of the animal experiments were performed in compliance with the IACUC ethical guidelines of the institution (Shanghai Institute of Materia Medica, Chinese Academy of Sciences, Shanghai; IACUC approval code 2018-05-ZJW-18). To investigate the pharmacokinetics of Dox-loaded HA-β-CD polymer, male SD rats (200 ± 20 g) were randomly divided into 2 groups (*n* = 5). Before administration, the rats fasted overnight but had free access to water. Free Dox or HA-β-CD-Dox were dosed via the jugular vein at a dose of 3 mg/kg equivalent to Dox. At the times of 5, 15, 30, 60, 120, 240, 360, 480, and 720 min, 200 µL of blood were collected from the jugular vein and centrifuged at 5000 rpm for 8 min to collect the plasma. Dox in the plasma was extracted through a deproteinization procedure. Briefly, 500 µL of acetonitrile (ACN) was added into 100 µL of plasma. The mixture was then vortexed and centrifuged for 10 min at 12,000g. The supernatants were transferred to new tubes and subjected to evaporation under vacuum using a concentrator. The residue was reconstituted in 100 µL of 30% ACN aqueous solution, in which Dox-<sup>13</sup>C, d<sub>3</sub> (0.05 µg mL<sup>-1</sup>) was added as an internal standard (IS) for quantification.

### 2.12. Drug distribution study

Female BALB/c-nu/nu mice (21–28 days) were used to evaluate the drug biodistribution after reaching the bodyweight of 15–18 g according to the following procedure. First, 100 µL of HeLa cells (1 × 10<sup>6</sup> cells/mL) were subcutaneously injected into the left flank of the mice. When the tumor volumes reached 70–100 mm<sup>3</sup>, the mice were randomly divided into two groups (3 mice/group): 1) In the Dox group the mice were injected with 3 mg kg<sup>-1</sup> of Dox; 2) In the HA-β-CD-Dox group, the mice were injected with HA-β-CD-Dox with Dox equivalent of 3 mg kg<sup>-1</sup>. All mice were sacrificed after 12 h. Afterward, the main organs (the livers, kidneys, hearts, spleens, lungs, and tumors) were removed from the

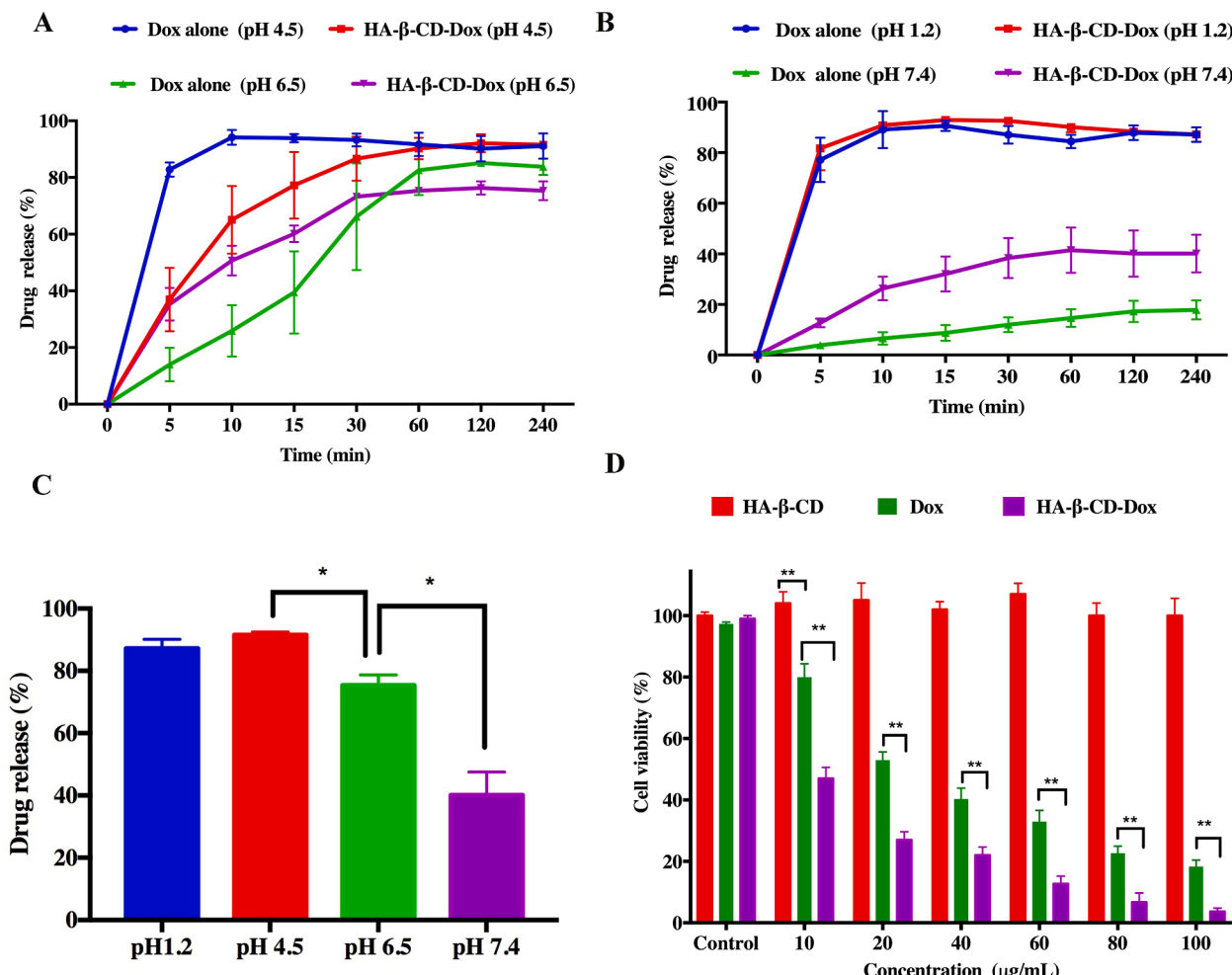


**Fig. 1.** The drug release profiles of Dox from HA-β-CD polymer (in contrast to free Dox) in buffers at (A) pH 4.5 and pH 6.5, and (B) pH 1.2 and pH 7.4. (C) The pH-responsive release of Dox from HA-β-CD polymer. (D) Cytotoxicity evaluation of HA-β-CD and HA-β-CD-Dox, in contrast to free Dox.  $n = 3$ ,  $p < 0.002$  (\*\*).

sacrificed mice, washed, and dried at ambient temperature. They were cut into small pieces using ophthalmic scissors and weighed; then 0.1 g of each tissue sample was placed in 96-well plates before the addition of 150  $\mu$ L of methanol and 50  $\mu$ L of DI water into each sample well before they were transferred into 1.5-mL Eppendorf tubes. Tissue homogenate samples were prepared by an ultrasonic cell crusher (Sonics Vibra-Cell; Sonics & Materials, Inc., Newtown, CT, USA) on ice with ultrasonic treatment (10 s/time 6 times with 5 s between intervals). The samples were then centrifuged at 12,000 rpm for 20 min. The supernatants were collected and stored at  $-80^{\circ}\text{C}$  until quantitative analysis using LC-MS/MS.

### 2.13. LC-MS/MS analysis

An AB SCIEX QTRAP® 6500 (Framingham, MA, USA) mass spectrometer with electrospray ionization source was interfaced with a Shimadzu high-performance liquid chromatography (HPLC) system. The analysis was performed using AB Sciex Analyst software (version 1.6.3) to control the liquid chromatography-tandem mass spectrometry system (LC-MS/MS). The separation was performed on a Shim-pack GISS C18 column, 100 mm  $\times$  2.1 mm ID, 1.9  $\mu\text{m}$  (Shimadzu, Kyoto, Japan) at a flow rate of 0.25 mL  $\text{min}^{-1}$ . The gradient started at 95% B for 0.5 min, linearly decreased to 3% B at 2 min, was held at 3% B for 4 min, increased to 95% B at 4.1 min, and held at 95% for 2 min. The mobile phase consisted of (A) 0.1% formic acid in acetonitrile and (B) 0.1% formic acid in H<sub>2</sub>O. The mass spectrometer was operated in a positive ion mode

with multiple reaction monitoring (MRM) for analysis. The MRM transitions were monitored at  $m/z$  544.3  $\rightarrow$  397.2 for doxorubicin and  $m/z$  548.2  $\rightarrow$  401.1 for the IS. Each sample was mixed with the IS solution before filtration, followed by LC-MS/MS quantification.

### 2.14. Statistical analysis

Data were expressed as mean values with standard deviation, one way ANOVA was used to compare two or multiple groups, and  $p < 0.05$  was considered significant.

## 3. Results and discussion

### 3.1. Synthesis and characterization

The polymer was synthesized as previously described (Singh et al., 2020). Herein, DPC forms crosslinks between two hydroxyl groups at high temperature and TEA acts as a nucleophilic catalyst that activates the carbonate ester and facilitates proton transfer, which forms a carbonate linkage between the hydroxyl groups of CD and HA (Fig. S1). The crude product required several washing steps to remove the reaction byproducts, such as phenol.

The molecular structure of the grafted polymer, HA-β-CD, was characterized using both SR-FTIR and <sup>1</sup>H NMR with all functional groups as expected based on our previous work (Singh et al., 2020) (Fig. S2A). Furthermore, we characterized the morphology and

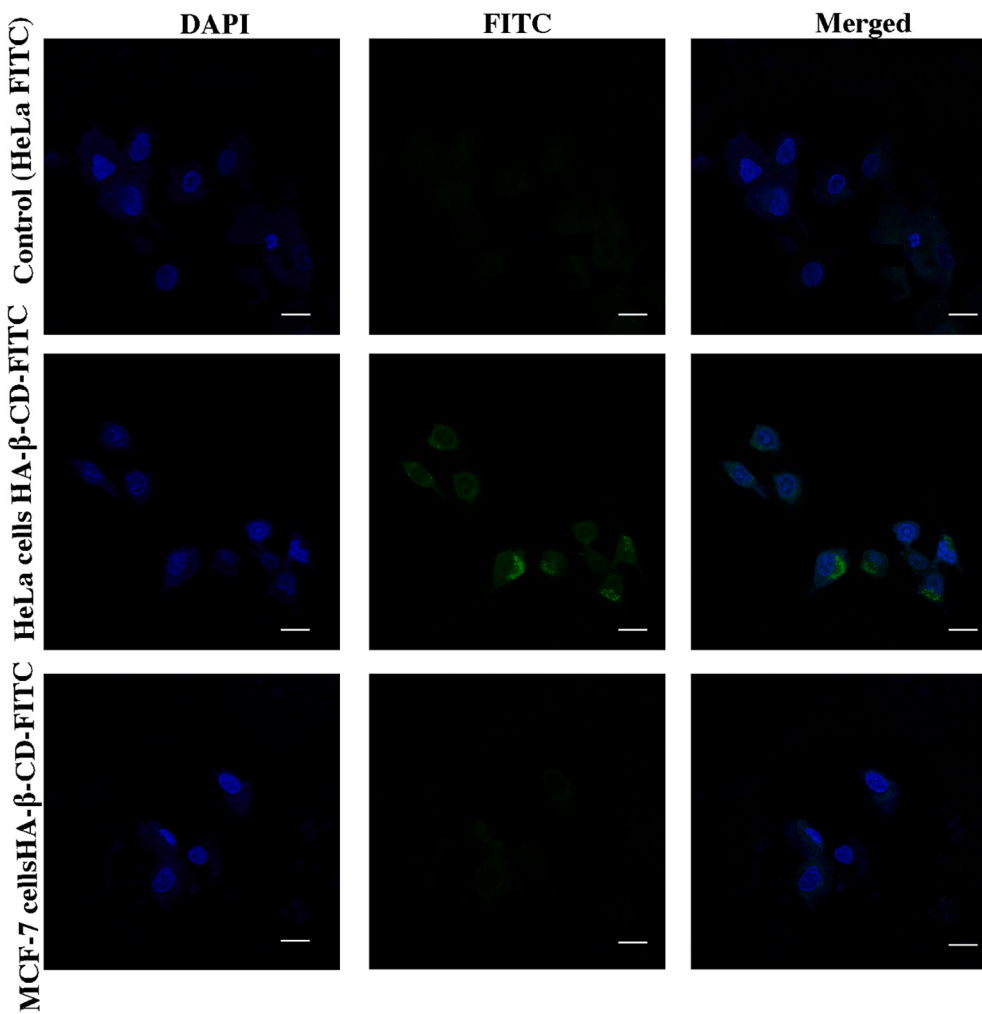


**Fig. 2.** Targeted delivery of a model drug FITC using HA- $\beta$ -CD in HeLa cells and MCF-7 cell models, showing the selective binding capability of HA- $\beta$ -CD to cells with CD44 receptors. Scale bar is 20  $\mu$ m.

structure of the HA- $\beta$ -CD polymer powder, because it is in particulate form in ethanol for drug loading. SEM analysis revealed the irregular morphology and porous structure of HA- $\beta$ -CD powder (Fig. S2B).  $\beta$ -CD has fair water solubility, but after combining with hydrophilic polymer HA, it became freely soluble in water, which was suitable for drug delivery and other biomedical applications. Water contact angle testing showed that the incorporation of  $\beta$ -CD increased the hydrophilicity of HA- $\beta$ -CD relative to HA, i.e.,  $40 \pm 4$  and  $60 \pm 4^\circ$ , respectively (Fig. S2C-D), thus enabling HA- $\beta$ -CD to deliver hydrophobic therapeutical agents by enhancing their water solubility.

To determine the size of the polymer, HPGPC analysis of the HA- $\beta$ -CD polymer was performed showing its homogenous composition with a single peak. The average molecular weights of HA and HA- $\beta$ -CD were  $\sim 27$  and  $50$  kDa, respectively (Fig. S3). Therefore, each HA backbone bore  $\sim 20$  CD units. To evaluate the specific surface area (SSA) and the pore texture of HA- $\beta$ -CD powder, BET analysis was performed. The adsorption/desorption isotherms, cumulative pore volume, and mean pore size obtained were calculated using the BJH method (McMillan and Teller, 1951) and results are depicted in Fig. S4. The sample was mesoporous with a specific surface area of  $3.05 \text{ m}^2 \text{ g}^{-1}$  (Bai et al., 2012; Riela et al., 2011).

### 3.2. Drug loading

To study the feasibility of using HA- $\beta$ -CD for drug delivery, a front-line chemotherapeutic drug, doxorubicin (Dox), was selected as a model

because its fluorescence enables cellular microscopic imaging. A well-validated HPLC method previously reported from our lab was used for quantitative analysis of drug loading (Singh et al., 2018). The average Dox loading capacity of HA- $\beta$ -CD was  $46.6 \pm 2.0 \text{ mg g}^{-1}$ , which is 9 times higher than for  $\beta$ -CD alone. This indicates that when  $\beta$ -CD molecules are grafted on the water-soluble polymer HA, they deliver Dox more efficiently, presumably because of contribution from the HA backbone that improved loading and unloading of drug cargo (Fig. S5). Similarly, when using Rhodamine B as a fluorescent model drug, we observed its loading capacity ( $31.1 \pm 1.7 \text{ mg g}^{-1}$ ) was 31 times higher than that in  $\beta$ -CD alone (Fig. S6).

### 3.3. pH-responsive drug release

To test if HA- $\beta$ -CD is suitable for targeted delivery of chemotherapeutics to cancerous tissues, we tested the pH effect on drug release because cancer tissues are slightly acidic ( $\text{pH} \sim 6.35\text{--}6.50$ ) and cell organelles responsible for drug uptake, such as endosomes, are  $\text{pH} \sim 4.5$  (Gerweck and Seetharaman, 1996; Raghunand and Gillies, 2000). Acidic pH enhanced drug release and maximum drug release was observed at  $\text{pH } 4.5$  in acetate buffer after  $\sim 1$  h (Fig. 1A). We further tested the drug release at the pH of human plasma (7.4) and gastric fluid (1.2). As shown in Fig. 1B, burst release of Dox was observed at acidic pH, whereas at pH 7.4 much less Dox was released. This pH-responsive drug release behavior is useful when designing a controlled drug delivery system based on HA- $\beta$ -CD that targets solid tumors because the cargo will be

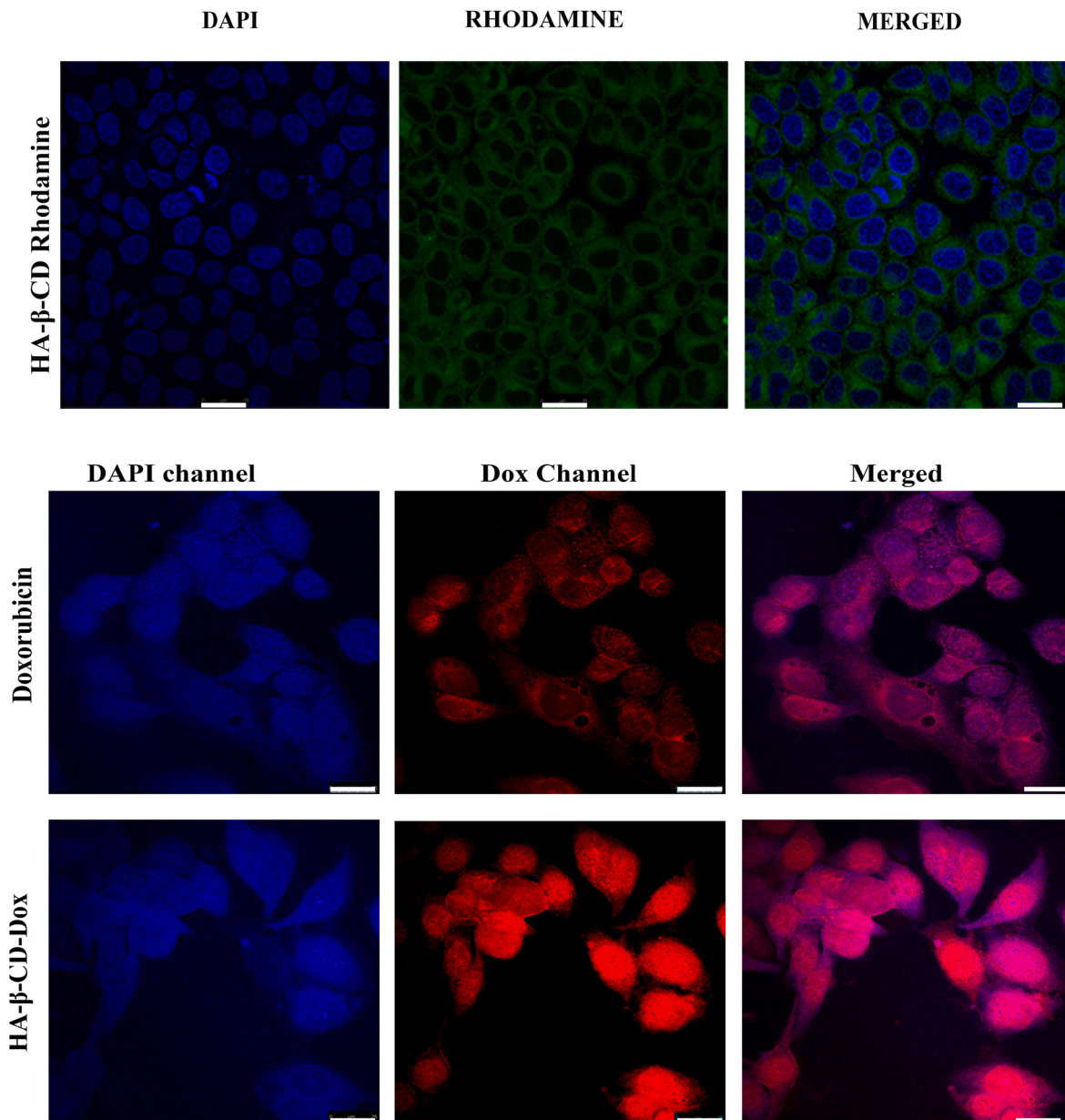


**Fig. 3.** The confocal laser scanning microscopy (CLSM) images of HeLa cells after 4 h of incubation with Rhodamine-B-loaded HA- $\beta$ -CD and Dox and Dox-loaded HA- $\beta$ -CD. The cell nuclei are stained with DAPI (blue fluorescence). Rhodamine B (green fluorescence) and Dox (red fluorescence) are visible. Scale bar is 25  $\mu$ m.

relatively stable in the bloodstream ( $\sim$ pH 7.4) but quickly released in the slightly acidic tumor microenvironment (Fig. 1C).

#### 3.4. Targeted drug delivery to tumor cell models

Biocompatibility is a prerequisite for use in drug delivery. Herein, HA- $\beta$ -CD exhibited high biocompatibility in cytotoxicity tests over different incubation times (Fig. 1D), which, in addition to its established biodegradability from previous research (Ji et al., 2017), meets the biocompatibility requirements for practical drug delivery applications. Importantly, Fig. 1D demonstrated much higher cytotoxicity of HA- $\beta$ -CD-Dox than Dox alone, even at the lowest concentration ( $10 \mu\text{g mL}^{-1}$ ). The enhanced cytotoxicity of HA- $\beta$ -CD-Dox was attributed to the enhanced cellular uptake of Dox via the cell receptor CD44 mediated cellular uptake as demonstrated in the following experiments.

Accordingly, we evaluated the feasibility of using HA- $\beta$ -CD for targeted drug delivery. The selective delivery of a drug by HA- $\beta$ -CD polymer to CD44 overexpressing cancer cells was demonstrated using FITC

as a model drug. Herein, two cell lines, HeLa cervical cancer and MCF-7 breast cancer, were used as cell models because they have different CD44 expression levels on their cell membranes. This was validated by fluorescence-activated cell sorting analysis (Fig. S7), where HeLa cells have significantly more CD44 receptors than MCF-7 cells. The confocal images showed FITC-loaded co-polymer selectively bound to HeLa cells in contrast to the negligible FITC fluorescence on MCF-7 cell surfaces indicating the CD44 targeting ability of HA- $\beta$ -CD (Fig. 2).

Further, two model drugs, e.g. Rhodamine B, a fluorescent dye, and Dox were used to illustrate the selective drug delivery efficacy of HA- $\beta$ -CD. Microscopic images show Rhodamine B surrounding the cell nuclei, indicating that Rhodamine B was incorporated within the cytoplasm, which was attributed to cell membrane CD44 receptor-mediated internalization (Park et al., 2014; Yu et al., 2013). In the Dox delivery experiment, a large amount of Dox accumulated in the cell nuclei after 4 h of incubation with HeLa cells, significantly more than the amount of Dox delivered without using HA- $\beta$ -CD (Fig. 3). Therefore, the results showed that the HA- $\beta$ -CD selectively bound to CD44 receptor that

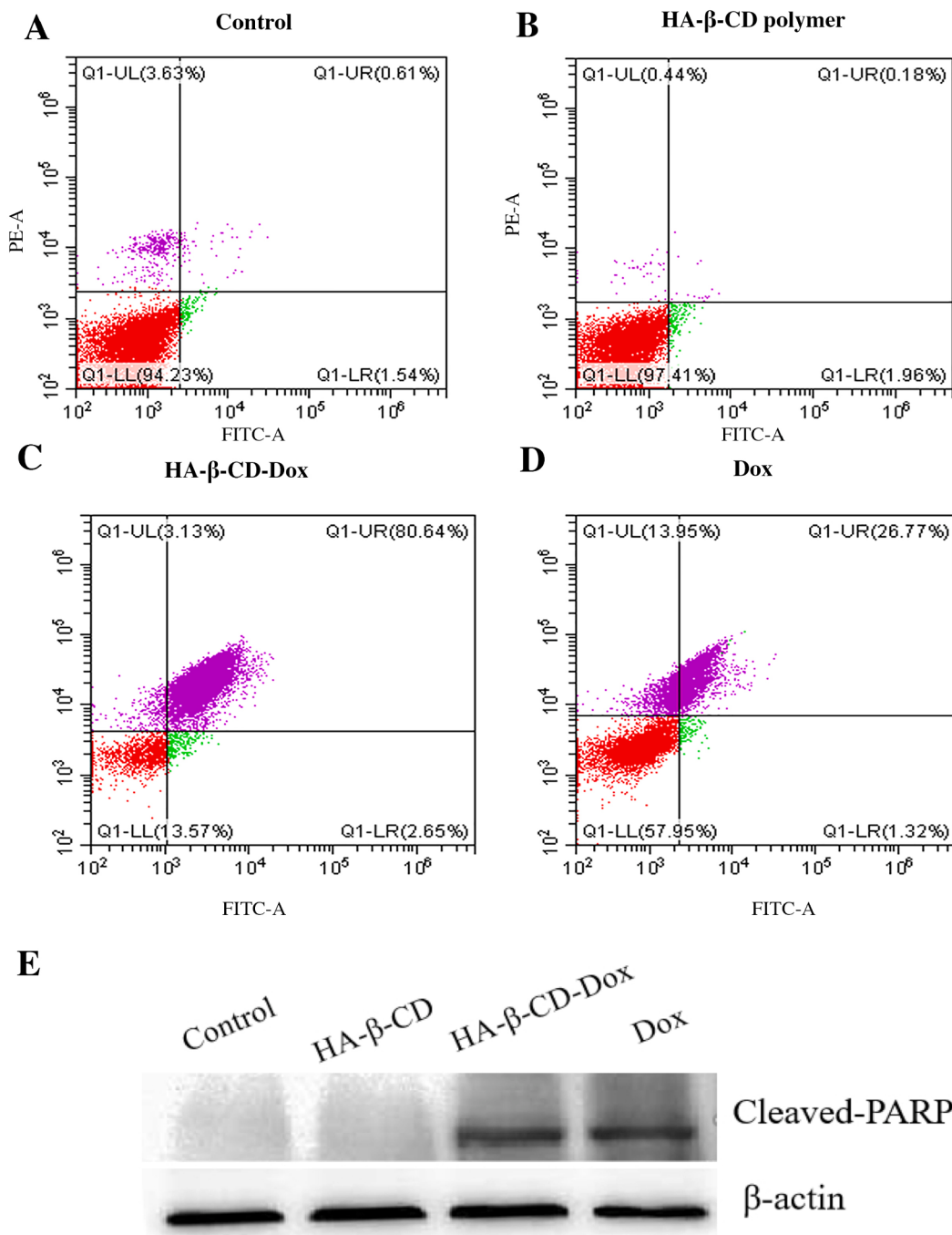


**Fig. 4.** Apoptosis analysis of HeLa cells when treated with HA- $\beta$ -CD, HA- $\beta$ -CD-Dox, and Dox. The HeLa cells were (A) untreated, i.e., control, or treated with (B) HA- $\beta$ -CD, (C) HA- $\beta$ -CD-Dox, and (D) Dox at the concentrations of 10  $\mu$ M for 24 h. (E) Western-blotting analysis of cleaved-PARP protein as the indicator of cell apoptosis, where  $\beta$ -actin was used as the gel loading control.

intermediated the Dox uptake and accumulation in cell nuclei. This data supports our hypothesis that the much higher cytotoxicity of HA- $\beta$ -CD-Dox than free dox was due to its enhanced cellular uptake of the polymer-drug complexes.

### 3.5. Apoptosis analysis

Annexin/PI staining based apoptosis analysis was performed in HeLa cells. The key factors for this analysis are the loss of membrane potential and phosphatidylserine externalization. The programmed (apoptosis) and non-programmed (necrosis) cell death induced by HA- $\beta$ -CD-Dox was evaluated by counting early apoptosis and late apoptosis. In Fig. 4, the

scatter plots are divided into four quadrants; living cells represented by lower left quadrant, early apoptosis represented by lower right quadrant, late apoptosis represented by upper right quadrant, and necrosis represented by upper left quadrant. HA- $\beta$ -CD induced nearly 2.2% apoptosis, comparable to that of untreated cells (~2.1%). In contrast, HA- $\beta$ -CD-Dox induced nearly 83.3% apoptosis which indicates a potent candidate for drug delivery applications, much higher than when treated by Dox alone (~28.1%).

The cell cycle distribution analysis was in line with the apoptosis analysis. As shown in Fig. 5, HA- $\beta$ -CD-Dox caused a higher SubG1 phase of HeLa cells (12.50%) than that of Dox alone (7.20%), while HA- $\beta$ -CD alone did not cause detectable SubG1, similar to PBS buffer (control),

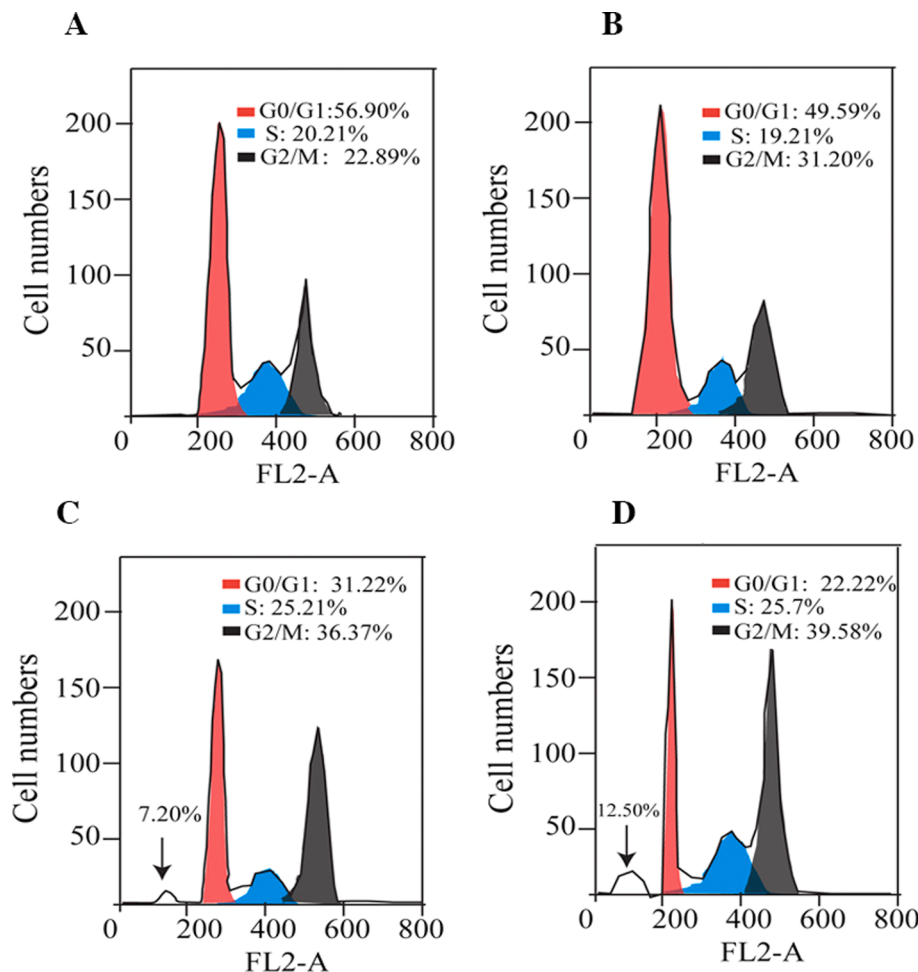


**Fig. 5.** Cell cycle analysis of HeLa Cells treated with (A) PBS as the negative control, (B) HA- $\beta$ -CD polymer, (C) Dox alone as a positive control, and (D) HA- $\beta$ -CD-Dox.

demonstrating that HA- $\beta$ -CD is a non-toxic but efficient drug carrier. To further substantiate the apoptosis results, we evaluated the expression of the cleavage of poly(ADP-ribose) polymerase (PARP) by caspase-3 during cell apoptosis, which is an established indicator of cell apoptosis. In line with the staining results (Fig. 5E), both HA- $\beta$ -CD-Dox and free Dox-induced PARP cleavage, in contrast to free HA- $\beta$ -CD and untreated cells (serving as the control) without PARP cleavage, further confirming HA- $\beta$ -CD by itself does not induce apoptosis and is thus promising as a biocompatible drug delivery vehicle. Noteworthily, the apoptosis results are consistent with that of the cytotoxicity evaluation of HA- $\beta$ -CD, HA- $\beta$ -CD-Dox, and free Dox in Fig. 1D.

### 3.6. Pharmacokinetic and biodistribution study

The plasma pharmacokinetic profiles of both HA- $\beta$ -CD-Dox and free Dox in rats display biphasic curves with a rapid decrease of initial plasma concentrations within 2 h (Fig. 6A). However, the HA- $\beta$ -CD-Dox showed slower drug clearance and significantly higher bioavailability, indicated by the area under the curve (AUC), than free Dox ( $p < 99\%$ ) with key parameters summarized in Table 1. Furthermore, the drug biodistribution study in the mice revealed a higher amount of Dox remained in the tumor tissue ( $314 \pm 55$ ) than free Dox ( $152 \pm 42$ ) after 12 h (Fig. 6B). Meanwhile, the polymer HA- $\beta$ -CD is capable of sustained drug delivery; after 12 h, there was still Dox in the blood in mice treated with HA- $\beta$ -CD-Dox; in contrast, no detectable Dox in the mouse blood treated with free Dox. In addition, in the free Dox treated mice, more Dox accumulated in the liver. Overall, all the data support that HA- $\beta$ -CD facilitated targeted delivery of Dox to the tumor tissue, sustained drug

release, and less liver toxicity.

### 4. Conclusions

Modification of biopolymers with advanced functionality is a very promising research area for biomedicine and the pharmaceutical industry. In this work, we have prepared a water-soluble supramolecular biopolymer HA- $\beta$ -CD with targeted drug delivery and controlled release properties. HA- $\beta$ -CD exhibits excellent biocompatibility, high drug loading capacity, pH-dependent drug release, and selective delivery of chemotherapeutics to CD44-overexpressed cancer cells, and is thus promising for targeted cancer therapy.

### CRediT authorship contribution statement

**Parbeen Singh:** Conceptualization, Methodology, Investigation.  
**Yongli Chen:** Cell experiments, In vivo study and Data processing.  
**Deependra Tyagi:** Validation.  
**Li Wu:** Software.  
**Xiaohong Ren:** Validation.  
**Jinglong Feng:** Software.  
**Andrew Carrier:** Manuscript preparation and editing.  
**Tiangang Luan:** Supervision.  
**Yongjun Tang:** Conceptualization, Supervision.  
**Jiwen Zhang:** Conceptualization, Supervision.  
**Xu Zhang:** Conceptualization, Supervision.

### Declaration of Competing Interest

The authors declare that they have no known competing financial interests or personal relationships that could have appeared to influence the work reported in this paper.

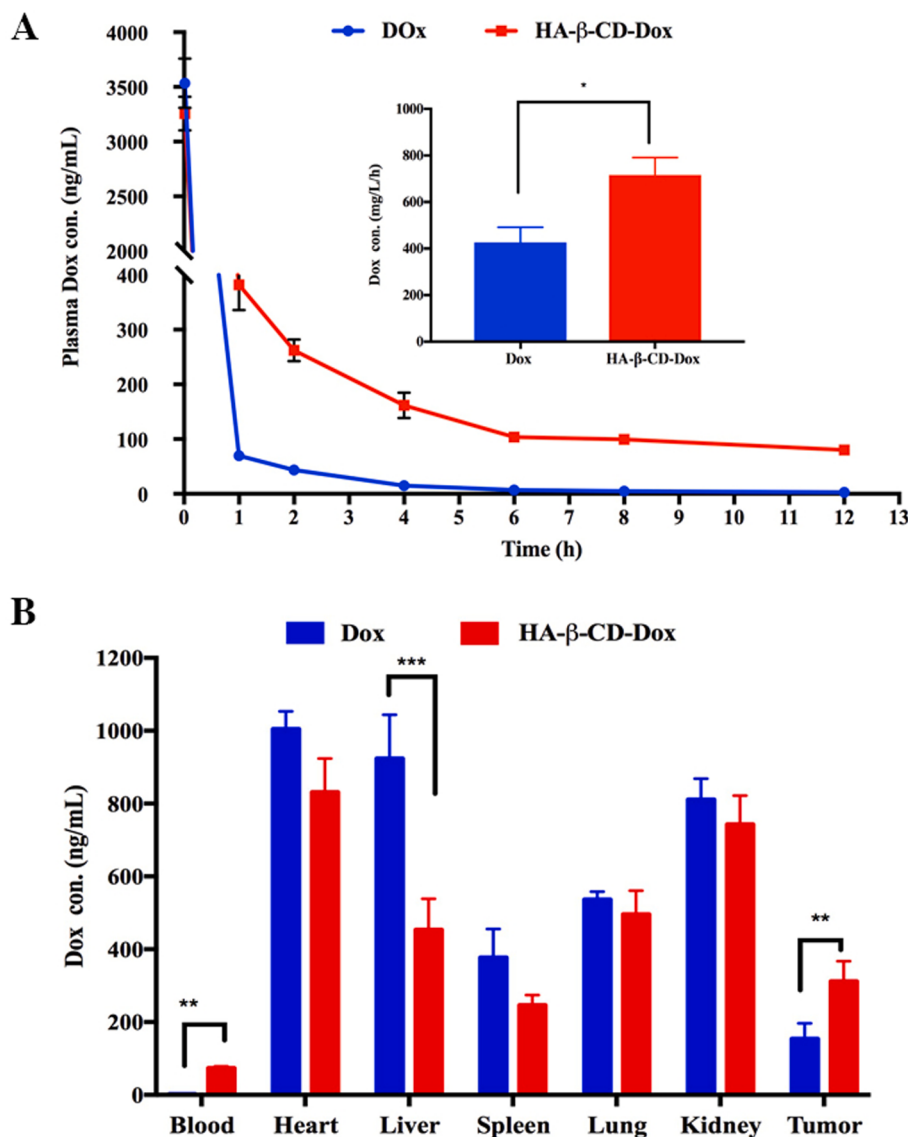


**Fig. 6.** (A) Blood plasma concentration of Dox in rats treated by HA-β-CD-Dox and free Dox ( $n = 5$ ). Inset: the  $AUC_{(0-t)}$  of Dox.  $p < 0.01$ (\*). (B) The biodistribution of Dox in the tumor tissue and main organs 12 h after intravenous injection of HA-β-CD-Dox and free Dox, where  $p < 0.002$  (\*\*) in the blood samples and tumor tissue and  $< 0.0001$  (\*\*\*) in the liver of the mice ( $n = 3$ ).

**Table 1**

The main pharmacokinetic parameters after intravenous administration of 3 mg kg<sup>-1</sup> Dox and Dox-loaded HA-β-CD polymer (mean  $\pm$  SD).

Parameters	Free Dox	HA-β-CD
$AUC_{(0-t)}$	mg L <sup>-1</sup> h <sup>-1</sup>	426 $\pm$ 65
$T_{1/2}$	h	0.3
$T_{max}$	h	0.12
$C_{max}$	ng mL <sup>-1</sup>	3533 $\pm$ 226
		3315 $\pm$ 108

#### Acknowledgments

The authors are grateful for the financial support from the Strategic Priority Research Program of the Chinese Academy of Sciences (XDA12050307), National Science and Technology Major Project (2017ZX09101001-006), Post-doctoral Foundation Project of Shenzhen Polytechnic (6019330006K, and 6019330007K), Shenzhen Science and Technology Program (GJHZ20180928161212140), Cape Breton University RISE program, NSERC Discovery Grants Program, and Canada Research Chairs program. We gratefully acknowledge the staff from

BL01B beamline of National Facility for Protein Science Shanghai (NFPS) at the Shanghai Synchrotron Radiation Facility Center for assistance during data collection.

#### Appendix A. Supplementary material

Supplementary data to this article can be found online at <https://doi.org/10.1016/j.ijpharm.2021.120602>.

#### References

- Ahrens, T., Sleeman, J.P., Schempp, C.M., Howells, N., Hofmann, M., Ponta, H., Herrlich, P., Simon, J.C., 2001. Soluble CD44 inhibits melanoma tumor growth by blocking cell surface CD44 binding to hyaluronic acid. *Oncogene* 20, 3399–3408.
- Bai, Y.X., Wang, J.P., Bashari, M., Hu, X.T., Feng, T., Xu, X.M., Jin, Z.Y., Tian, Y.Q., 2012. A thermogravimetric analysis (TGA) method developed for estimating the stoichiometric ratio of solid-state alpha-cyclodextrin-based inclusion complexes. *Thermochim Acta* 541, 62–69.
- Charlot, A., Heyraud, A., Guenot, P., Rinaudo, M., Auzély-Velty, R., 2006. Controlled synthesis and inclusion ability of a hyaluronic acid derivative bearing β-cyclodextrin molecules. *Biomacromolecules* 7, 907–913.

- Choi, K.Y., Yoon, H.Y., Kim, J.-H., Bae, S.M., Park, R.-W., Kang, Y.M., Kim, I.-S., Kwon, I.C., Choi, K., Jeong, S.Y., Kim, K., Park, J.H., 2011. Smart nanocarrier based on PEGylated hyaluronic acid for cancer therapy. *ACS Nano* 5, 8591–8599.
- Crini, G., 2014. Review: a history of cyclodextrins. *Chem. Rev.* 114, 10940–10975.
- Davis, M.E., Brewster, M.E., 2004. Cyclodextrin-based pharmaceutics: past, present and future. *Nat. Rev. Drug Discov.* 3, 1023–1035.
- Ekladious, I., Colson, Y.L., Grinstaff, M.W., 2019. Polymer-drug conjugate therapeutics: advances, insights and prospects. *Nat. Rev. Drug Discovery* 18, 273–294.
- Entwistle, J., Hall, C.L., Turley, E.A., 1996. Receptors: Regulators of signalling to the cytoskeleton. *J. Cell. Biochem.* 61, 569–577.
- Gerweck, L.E., Seetharaman, K., 1996. Cellular pH gradient in tumor versus normal tissue: potential exploitation for the treatment of cancer. *Cancer Res.* 56, 1194–1198.
- Hall, C.L., Yang, B.H., Yang, X.W., Zhang, S.W., Turley, M., Samuel, S., Lange, L.A., Wang, C., Curpen, G.D., Savani, R.C., Greenberg, A.H., Turley, E.A., 1995. Overexpression of the hyaluronan receptor rhamm is transforming and is also required for H-ras transformation. *Cell* 82, 19–28.
- Herrlich, P., Sleeman, J., Wainwright, D., Konig, H., Sharman, L., Hilberg, F., Ponta, H., 1998. How tumor cells make use of CD44. *Cell Adhes. Commun.* 6, 141–147.
- Hua, Q., Knudson, C.B., Knudson, W., 1993. Internalization of hyaluronan by chondrocytes occurs via receptor-mediated endocytosis. *J. Cell Sci.* 106, 365–375.
- Ji, Y., Shan, S., He, M., Chu, C.-C., 2017. Inclusion complex from cyclodextrin-grafted hyaluronic acid and pseudo protein as biodegradable nano-delivery vehicle for gambogic acid. *Acta Biomater.* 62, 234–245.
- Knudson, C.B., Knudson, W., 1993. Hyaluronan-binding proteins in development, tissue homeostasis, and disease. *FASEB J.* 7, 1233–1241.
- Langer, R., Vacanti, J.P., 1993. Tissue engineering. *Science* 260, 920–926.
- Laurent, T., 1989. The biology of hyaluronan - introduction. *Ciba F Symp* 143, 1–5.
- Lee, H., Ahn, C.H., Park, T.G., 2009. Poly[lactic-co-(glycolic acid)]-grafted hyaluronic acid copolymer micelle nanoparticles for target-specific delivery of doxorubicin. *Macromol. Biosci.* 9, 336–342.
- Lee, M.Y., Park, S.J., Park, K., Kim, K.S., Lee, H., Hahn, S.K., 2011. Target-specific gene silencing of layer-by-layer assembled gold-cysteamine/siRNA/PEI/HA nanocomplex. *ACS Nano* 5, 6138–6147.
- Li, Z., Song, N., Yang, Y.-W., 2019. Stimuli-responsive drug-delivery systems based on supramolecular nanovalves. *Matter* 1, 345–368.
- Liechty, W.B., Kryscio, D.R., Slaughter, B.V., Peppas, N.A., 2010. Polymers for drug delivery systems. *Ann. Rev. Chem. Biomol. Eng.* 1, 149–173.
- Liu, Q., Das, M., Liu, Y., Huang, L., 2018. Targeted drug delivery to melanoma. *Adv. Drug Deliv. Rev.* 127, 208–221.
- Lv, S., Dudek, D.M., Cao, Y., Balamurali, M.M., Gosline, J., Li, H.B., 2010. Designed biomaterials to mimic the mechanical properties of muscles. *Nature* 465, 69–73.
- Mao, Y.-H., Song, A.-X., Yao, Z.-P., Wu, J.-Y., 2018. Protective effects of natural and partially degraded konjac glucomannan on Bifidobacteria against antibiotic damage. *Carbohydr. Polym.* 181, 368–375.
- McMillan, W.G., Teller, E., 1951. The assumptions of the B.E.T. Theory. *J. Phys. Chem.* 55, 17–20.
- Miraftab, R., Xiao, H., 2019. Feasibility and potential of graphene and its hybrids with cellulose as drug carriers: a commentary. *J. Bioreour. Bioprod.* 4, 200–201.
- Namgung, R., Mi Lee, Y., Kim, J., Jang, Y., Lee, B.-H., Kim, I.-S., Sokkar, P., Rhee, Y.M., Hoffman, A.S., Kim, W.J., 2014. Poly-cyclodextrin and poly-paclitaxel nano-assembly for anticancer therapy. *Nat. Commun.* 5, 3702.
- Orive, G., Anita, E., Pedraz, J.L., Emerich, D.F., 2009. Biomaterials for promoting brain protection, repair and regeneration. *Nat. Rev. Neurosci.* 10, 682–U647.
- Park, J.-H., Cho, H.-J., Yoon, I.-S., Ko, S.-H., Shim, J.-S., Cho, J.-H., Park, J. H., Kim, K., Kwon, I.C., Kim, D.-D., 2014. Hyaluronic acid derivative-coated nanohybrid liposomes for cancer imaging and drug delivery. *J. Control. Release* 174, 98–108.
- Raghunand, N., Gillies, R.J., 2000. pH and drug resistance in tumors. *Drug Resist. Updates* 3, 39–47.
- Riela, S., Lazzara, G., Lo Meo, P., Guernelli, S., D'Anna, F., Milioto, S., Noto, R., 2011. Microwave-assisted synthesis of novel cyclodextrin-cucurbituril complexes. *Supramol. Chem.* 23, 819–828.
- Singh, P., Ren, X., Guo, T., Wu, L., Shakya, S., He, Y., Wang, C., Maharjan, A., Singh, V., Zhang, J., 2018. Biofunctionalization of β-cyclodextrin nanosplices using cholesterol. *Carbohydr. Polym.* 190, 23–30.
- Singh, P., Wu, L., Ren, X., Zhang, W., Tang, Y., Chen, Y., Carrier, A., Zhang, X., Zhang, J., 2020. Hyaluronic-acid-based β-cyclodextrin grafted copolymers as biocompatible supramolecular hosts to enhance the water solubility of tocopherol. *Int. J. Pharm.* 586, 119542.
- Soltés, L., Mendichi, R., Machová, E., Steiner, B., Alföldi, J., Sasinková, V., Bystríký, S., Balog, K., 1999. Cyclodextrin derivative of hyaluronan. *Carbohydr. Polym.* 39, 17–24.
- Wang, C., Ye, Y., Hochu, G.M., Sadeghifar, H., Gu, Z., 2016. Enhanced cancer immunotherapy by microneedle patch-assisted delivery of anti-PD1 antibody. *Nano Lett.* 16, 2334–2340.
- Webber, M.J., Appel, E.A., Meijer, E.W., Langer, R., 2016. Supramolecular biomaterials. *Nat. Mater.* 15, 13–26.
- Webber, M.J., Khan, O.F., Sydlik, S.A., Tang, B.C., Langer, R., 2015. A perspective on the clinical translation of scaffolds for tissue engineering. *Ann. Biomed. Eng.* 43, 641–656.
- Xiao, Y., Chinoy, Z.S., Pecastaings, G., Bathany, K., Garanger, E., Lecommandoux, S., 2020. Design of polysaccharide-b-elastic-like polypeptide bioconjugates and their thermoresponsive self-assembly. *Biomacromolecules* 21, 114–125.
- Yan, J.-K., Wang, Y.-Y., Qiu, W.-Y., Wu, J.-Y., 2017. Construction and characterization of nanosized curdlan sulfate/chitosan polyelectrolyte complex toward drug release of zidovudine. *Carbohydr. Polym.* 174, 209–216.
- Yu, M., Jambhrunkar, S., Thorn, P., Chen, J., Gu, W., Yu, C., 2013. Hyaluronic acid modified mesoporous silica nanoparticles for targeted drug delivery to CD44-overexpressing cancer cells. *Nanoscale* 5, 178–183.
- Zhou, J.W., Ritter, H., 2010. Cyclodextrin functionalized polymers as drug delivery systems. *Polym. Chem.-Uk* 1, 1552–1559.